

A survey of weak stability boundaries in the Sun-Mars system *

Jian Li and Yi-Sui Sun

School of Astronomy and Space Science & Key Laboratory of Modern Astronomy and Astrophysics in Ministry of Education, Nanjing University, Nanjing 210093, China;
ljian@nju.edu.cn

Received 2013 November 4; accepted 2014 June 20

Abstract We investigate the weak stability boundary (WSB) for a new primary, Mars, in the framework of the planar circular restricted 3-body problem, and also in the planar bicircular restricted 4-body problem by including a perturbation due to Jupiter. For the sake of a simple stability/instability criterion, our computations have been done using the equations of motion in polar coordinates. It is found that the relative size of the weakly stable sets around Mars is much larger than that of the Earth-Moon and the Sun-Jupiter systems, as the mass ratio of the Sun-Mars system is significantly smaller. We propose that this difference could be scaled by the Hill radius. In an enlarged view of the domain close to Mars, the geometry of the WSB has been presented for various parameters and compared to previous works. Our results also show that Jupiter's gravitational force would strongly affect the Martian stable regions and should be taken into account to design a ballistic capture trajectory.

Key words: celestial mechanics

1 INTRODUCTION

The transfer trajectory of a spacecraft from the Earth to the Moon is generally constructed by the well known Hohmann transfer (Hohmann 1925; Bate et al. 1971). In this transfer technique, the semimajor axis of the spacecraft about the Earth is increased by the first maneuver ΔV_1 , with apogee reaching the lunar orbit. Upon arrival at the apogee of the transfer orbit, the second maneuver ΔV_2 is applied to the spacecraft in order that the Keplerian energy with respect to the Moon becomes negative, so that a Moon-centered elliptic orbit is obtained. This ΔV_2 implies that a substantial amount of fuel is needed to slow down the spacecraft for capture into a parking orbit around the Moon.

A new type of Earth-to-Moon transfer was invented by Belbruno (1987) and Belbruno & Miller (1993) based on the weak stability boundary (WSB). The motivation for these transfers is to design a trajectory for the spacecraft to automatically reach lunar orbit without the use of rocket engines to brake, which is termed ballistic capture. The WSB transfer is a low energy process since no fuel would be required in the lunar capture (i.e. $\Delta V_2 = 0$). This is a remarkable property that distinguishes it from the classical Hohmann transfer. Belbruno & Carrico (2000) compared these two kinds of transfers in detail, showing that the WSB transfer can save as much as 25% of the energy;

* Supported by the National Natural Science Foundation of China.

but the spacecraft will take about 90 days to arrive at the Moon instead of the standard three days. It is important to note that the WSB transfer is not only of practical interest but also of theoretical interest. As pointed out by Belbruno et al. (2010) in the context of the planar circular restricted 3-body problem, the stable manifolds of Lyapunov orbits about Lagrangian equilibrium points L_1 and L_2 are associated with the WSB for a significant range of energies. Therefore, the WSB may act as a good substitute for hyperbolic invariant manifolds in the study of dynamics around a small primary.

The concept of the WSB transfer was first applied to redesign the trajectory of the Japanese mission *Hiten* in 1991, and maneuver the spacecraft into an orbit around the Moon with the very little fuel that it had left (Belbruno & Miller 1990). This success demonstrated the very advantage of utilizing the methods of astrodynamics. In another application, WSB methodology was also used to design a low-energy lunar transfer for the spacecraft *SMART-1* of the European Space Agency (ESA) in 2004 (Schoenmaekers et al. 2001). Currently, ESA plans to send *BepiColombo* to explore the planet Mercury in 2015. Considering the high approach excess hyperbolic velocity of $\sim 300 \text{ m s}^{-1}$ with respect to Mercury, a traditional chemical orbit insertion burn by the engine may fail and the mission would be lost. To avoid such a single-point failure, a WSB capture trajectory has been proposed (Jehn et al. 2004).

There is a considerable amount of literature devoted to mathematical definitions of WSB (Belbruno & Miller 1990; Belbruno 2002; Yagasaki 2004a,b), although they are neither precise enough nor suitable for visualization. The algorithmic definition of the WSB can be found in Belbruno (2004), in the framework of the Earth-Moon-spacecraft restricted 3-body model. The boundary can be viewed as a location r^* along the radial line l from the Moon where the first transition between weakly stable and unstable motion occurs. The stable/unstable motion refers to the case that the spacecraft can/cannot perform a full cycle about the Moon without going around the Earth. After this definition was proposed, García & Gómez (2007) generalized the WSB region by considering the fact that there are actually multiple transitions from stability to instability for a lunar distance larger than r^* . They claimed that the geometry of WSB is much more complicated than that in Belbruno (2002), since there is not a single location defining the WSB on each segment l . Moreover, they further examined the n -stable trajectory, which makes n full cycles around the Moon. Using the refined definition in García & Gómez (2007), Topputo & Belbruno (2009) investigated the WSB for another case of the Sun-Jupiter system. They found that the variability of the mass ratio of the primaries, relative to the Earth-Moon case, has an important effect of changing the structure of the weakly stable sets. More recently, the applicability of the WSB sets within the lunar Hill sphere in view of the low-energy transfer from the Earth to the Moon has been carefully tested by Sousa Silva & Terra (2012a,b), and they showed how to select stable subsets which can provide feasible ballistic captures, e.g. excluding collisional trajectories.

The general goal of the present paper is to draw the new geometry of the WSB in the Sun-Mars system, which has not been published yet and is also of particular interest in some upcoming space missions. In contrast to the cases of Earth-Moon and Sun-Jupiter considered in previous studies, the mass ratio of the Sun-Mars system is four to five orders of magnitude smaller. In this way, we would obtain a more comprehensive understanding of the WSB for a wider class of circular restricted 3-body systems, since the mass ratio is the only parameter in their equations of motion. Furthermore, we take into account the influence of Jupiter on the spacecraft, and the more realistic stable sets around Mars could be obtained. In order to fulfill these computations, we extend the equations of motion in polar coordinates defined by García & Gómez (2007) to the bicircular restricted 4-body model. Finally, it has to be remarked that in the widely-used approach, the excess hyperbolic velocity associated with Mars is quite high, equivalent to that of Mercury, thus the WSB strategy could be adopted to design an ideal transfer trajectory.

The remainder of this paper is organized as follows. Section 2 describes the motion of the spacecraft in the three and four body models. The algorithmic definition of the WSB is given in Section 3. In Section 4, for ease of determining the stable/unstable points, we rewrite the equations of motion in

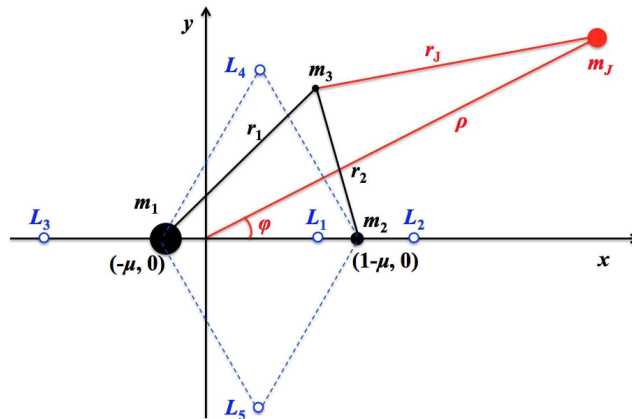


Fig. 1 The synodic coordinate system (x, y) , showing the locations of the Sun (m_1), Mars (m_2), the spacecraft (m_3) and Jupiter (m_J). The Lagrangian equilibrium points of the Sun-Mars system in the framework of the PCR3BP are denoted by L_i ($i = 1, 2, 3, 4, 5$).

polar coordinates; and the weakly stable regions around Mars are numerically computed for different parameters. The conclusions and discussion are presented in Section 5.

2 EQUATIONS OF MOTION

In this section, we first introduce the Planar Circular Restricted 3-Body Problem (PCR3BP) that will be used to study the WSB (see Fig. 1). In the framework of the PCR3BP, we consider the motion of a massless particle m_3 moving under the gravitational perturbations of two primary bodies m_1 and m_2 in the same plane. We assume that m_1 and m_2 have Keplerian circular orbits about their common center of mass, and they exert forces on the particle m_3 but are not affected by m_3 . In this paper, the three bodies m_1, m_2 and m_3 represent the Sun, Mars and a spacecraft, respectively.

Since m_1 and m_2 are moving on circular orbits, then they have a constant angular velocity $n = 2\pi/P$, where P is their common orbital period. We adopt the synodic coordinate system (x, y) that has its origin located at the center of mass of the two primaries, and rotates at a uniform rate n . In such a system, m_1 and m_2 always lie on the x -axis. It is customary to choose the total mass $(m_1 + m_2)$, the mutual distance between the Sun and Mars, and the gravitational constant G to all be 1. According to Kepler’s third law of planetary motion, we have $P = 2\pi$, i.e. $n = 1$. Let the mass ratio $\mu = m_2/(m_1 + m_2)$, then m_1 can be fixed at $(x_1, y_1) = (-\mu, 0)$ and m_2 is placed at $(x_2, y_2) = (1 - \mu, 0)$. For the Sun-Mars case, we will restrict ourselves to $\mu = m_2/(m_1 + m_2) = 3.2271504036 \times 10^{-7}$ in the following.

Let the coordinates of the spacecraft m_3 in the synodic system be (x, y) , then the equations of motion are described by

$$\begin{aligned} \ddot{x} - 2\dot{y} &= \frac{\partial U}{\partial x}, \\ \ddot{y} + 2\dot{x} &= \frac{\partial U}{\partial y}, \end{aligned} \tag{1}$$

where the “pseudo-potential” $U = U(x, y)$ is given by

$$U = \frac{1}{2}(x^2 + y^2) + \frac{1-\mu}{r_1} + \frac{\mu}{r_2} + \frac{1}{2}\mu(1-\mu), \tag{2}$$

with

$$\begin{aligned} r_1^2 &= (x + \mu)^2 + y^2, \\ r_2^2 &= (x + \mu - 1)^2 + y^2. \end{aligned} \quad (3)$$

The system of differential equations given in Equation (1) has the well known Jacobi constant (or Jacobi integral)

$$C(x, y, \dot{x}, \dot{y}) = 2U(x, y) - (\dot{x}^2 + \dot{y}^2). \quad (4)$$

The greatest usefulness of the Jacobi constant is associated with the locations where the velocity of m_3 is equal to zero, i.e.

$$C = 2U(x, y) = (x^2 + y^2) + 2 \left(\frac{1 - \mu}{r_1} + \frac{\mu}{r_2} \right) + \mu(1 - \mu), \quad (5)$$

which determines a set of curves in the x - y plane for particular values of C . This is the concept of zero-velocity curves. It is obvious that Equation (4) requires $2U \geq C$ since otherwise the velocity would be complex. Thus a zero-velocity curve defines the boundary between permissible and forbidden regions in the motion of m_3 .

The motion described by Equation (1) has five equilibrium points, where m_3 has zero velocity ($\dot{x} = \dot{y} = 0$) and zero acceleration ($\ddot{x} = \ddot{y} = 0$) in the rotating frame. As shown in Figure 1, the three collinear Lagrangian equilibrium points L_1 , L_2 and L_3 lie along the x -axis; there are two triangular Lagrangian equilibrium points L_4 and L_5 , each of which forms an equilateral triangle with the primaries m_1 and m_2 . The topology of zero-velocity curves in the PCR3BP will change when C passes through its critical values computed at these five Lagrangian equilibrium points. The largest critical value of C is attained at the L_1 point, and it can be expressed in terms of μ (Murray & Dermott 1999)

$$C_{L_1} \approx 3 + 3^{4/3} \mu^{2/3} - 10\mu/3. \quad (6)$$

If the Jacobi constant $C > C_{L_1}$ then the region of possible motion for m_3 is divided into three disjoint parts: one around m_1 , one around m_2 and the other at a large distance. In this case the WSB transfer of the spacecraft going from a long distance (e.g. near the Earth) to the vicinity of Mars is not likely to take place, because to do so the spacecraft would have to cross the zero-velocity curves and travel in the forbidden region of motion.

Next, we include the gravitational force of the giant neighbor of Mars – Jupiter – on the spacecraft by means of the Planar Bicircular Restricted 4-Body Problem (PBR4BP). The framework to deal with it is the same the synodic system as in the PCR3BP (Fig. 1), where the Sun and Mars are rotating around their center of mass, while Jupiter is supposed to be turning clockwise in a circle about the Sun-Mars barycenter. The four bodies are assumed to move in the same plane. Then in PBR4BP, the motion of the spacecraft m_3 is governed by the modified set of second order differential equations

$$\begin{aligned} \ddot{x} - 2\dot{y} &= \frac{\partial(U + \Omega)}{\partial x}, \\ \ddot{y} + 2\dot{x} &= \frac{\partial(U + \Omega)}{\partial y}, \end{aligned} \quad (7)$$

with the terms related to Jupiter being

$$\begin{aligned} \Omega &= \frac{m_J}{r_J} - \frac{m_J}{\rho^2} (x \cos \phi + y \sin \phi), \\ r_J^2 &= (x - \rho \cos \phi)^2 + (y - \rho \sin \phi)^2, \\ \phi &= \phi(t) = \omega_J \cdot t + \phi_0, \end{aligned} \quad (8)$$

where r_J is the distance between the spacecraft and Jupiter, ϕ is the phase angle between Jupiter and the Sun-Mars direction (i.e. the positive direction of the x -axis), and the constant ϕ_0 corresponds to the initial value of ϕ at $t = 0$. Referring to the adimensional units as in the case of PCR3BP, we take $m_J = 9.5479163030 \times 10^{-4}$ to be the mass of Jupiter, $\rho = 3.4156295646$ as the distance between Jupiter and the Sun-Mars barycenter, and $\omega = -0.8415102846$ as the relative angular velocity in the rotating coordinate system.

The PBR4BP is a good approximate model for the Sun-Mars-Jupiter system, since Mars's eccentricity is about 0.093 and Jupiter's is about 0.048, and the inclination between the orbits of these two planets is less than 1° . However, it should be noticed that the system defined by Equation (7) no longer admits either the Jacobi constant or equilibrium points like the one given by Equation (1) does.

3 DEFINITION OF THE WEAK STABILITY BOUNDARY

In order to define the WSB according to Belbruno (2004), it is necessary to give the two-body Keplerian energy H_2 of the spacecraft m_3 with respect to Mars m_2 . Let v be the magnitude of the velocity of m_3 in m_2 -centered inertial coordinates, then we have

$$H_2 = \frac{1}{2}v^2 - \frac{\mu}{r_2}, \tag{9}$$

where r_2 is the distance from m_3 to m_2 and has been given in Equation (3).

In the framework of the PCR3BP, we will give the algorithmic definitions of the weakly stable set W and the WSB ∂W . Consider all the trajectories of m_3 with such initial conditions (Fig. 2):

- (i) The initial position of the trajectory is on a radial segment $l(\theta)$ departing from Mars m_2 and making an angle θ with respect to the x -axis, in the rotating system. The motion of m_3 is assumed to start at the periapsis of an osculating ellipse with respect to m_2 with eccentricity e , i.e. the initial velocity vector of m_3 is normal to the line l . This is

$$v(0) = \sqrt{\frac{\mu(1+e)}{r}}, \tag{10}$$

where $r = r_2(0)$ is the initial radius. It should be stated that there are two different choices for the direction of the initial velocity, prograde motion and retrograde motion. In this paper, only the prograde one will be investigated since such a trajectory is of great interest in the design of WSB transfers.

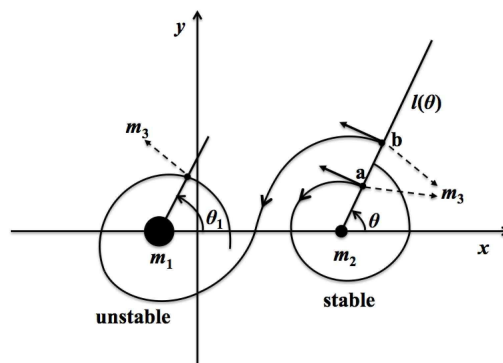


Fig. 2 The algorithmic definition of stable and unstable orbits of m_3 .

- (ii) The initial Keplerian energy $H_2(0)$ is negative at $t = 0$. By virtue of Equations (9) and (10), we obtain

$$H_2(0) = \frac{\mu}{2} \cdot \frac{e-1}{r}. \quad (11)$$

So, it is obvious that the requirement $H_2(0) < 0$ on the initial conditions is equivalent to $e \in [0, 1)$.

- (iii) The eccentricity e of the initial osculating ellipse around m_2 is constant along the line l . Then after fixing the angle θ , the evolution of m_3 only depends on the initial distance r . The value of $v(0)$ can be deduced from Equation (10) and it varies along l .

Suppose that m_3 starts its motion with the above initial conditions. We define weak stability and instability in the following way (Belbruno 2004; Romagnoli & Circi 2009).

Definition 1 The motion of m_3 is said to be weakly n -stable if after leaving the point $a \in l$, it makes n full cycles about m_2 without going around m_1 (Fig. 2), and it has negative or zero Keplerian energy H_2 relative to m_2 for every return to the line l .

Definition 2 The motion of m_3 is weakly n -unstable if:

- (1) after leaving the line l , the forward trajectory of m_3 intersects l again at a point where the Keplerian energy H_2 is positive, without going around m_1 ;
- (2) after leaving the point $b \in l$, m_3 moves away from m_2 towards m_1 and performs a complete turn around m_1 before its n -th return to l (Fig. 2);
- (3) after leaving the line l , m_3 collides with either of the two primaries, m_1 or m_2 .

Condition (1) of the weak instability is the ballistic escape and condition (2) is generally called the primary interchange escape. To exclude condition (3) for a relatively large stability number n , we may be able to construct safe capture trajectories in practical applications.

In the PCR3BP, the existence of the Jacobi constant does permit us to find the n -stable regime in a sufficiently small open neighborhood of m_2 . For the spacecraft m_3 having Jacobi constant $C > C_{L_1}$, if it is originally orbiting around m_2 with small r , then it can never escape towards m_1 . Otherwise, m_3 would have to cross the forbidden region where the motion is impossible. Stability against escape for this case is essentially Hill stability (Hill 1878; Szebehely 1978). However, as the initial conditions vary along the line l satisfying (i)–(iii), there is a critical distance $r^*(\theta, e) \in l$ from m_2 having the following properties:

- if $r \leq r^*$, the motion is n -stable;
- if $r > r^*$, the motion is n -unstable.

Then the WSB can be defined as (Belbruno 2004)

$$\partial W_n^* = \{r^*(\theta, e) | \theta \in [0, 2\pi], e \in [0, 1)\}, \quad (12)$$

where r^* is a smooth function of θ and e , and it indicates the *first* transition from stability to instability.

Furthermore, the definition of the WSB given by the set in Equation (12) has been generalized by García & Gómez (2007). They showed that, for values of the initial radius larger than r^* , there are still a finite number of points r_k^* along the line l for which stable/unstable transitions would also occur. Then the weakly n -stable points on l can be given by a countable union of closed intervals

$$W_n(\theta, e) = \bigcup_{k \geq 1} [r_{2k-1}^*, r_{2k}^*], \quad (13)$$

where $r_{k \geq 2}^*$ depends on θ and e , and the precision of numerical calculations. Here, we denote r_1^* as the physical radius of Mars, and r_2^* as the prescribed critical distance r^* corresponding to the single transition.

By varying the counterclockwise angle $\theta \in [0, 2\pi]$ measured from the positive direction of the x -axis and the eccentricity $e \in [0, 1)$ of the initial osculating ellipse, we have the following weakly stable sets of order n :

$$W_n(e) = \bigcup_{\theta \in [0, 2\pi]} W_n(\theta, e), \tag{14}$$

and

$$W_n = \bigcup_{\theta \in [0, 2\pi], e \in [0, 1)} W_n(e). \tag{15}$$

As observed in García & Gómez (2007), W_n is a complicated region that recalls a Cantor set and has a fractional dimension between 2 and 3.

According to the above description of stable sets, if $r \in [r_{2k-1}^*, r_{2k}^*]$ the motion is n -stable, and for any arbitrarily small δ , all points $r' \in [r_{2k}^* + \delta, r_{2k+1}^* - \delta]$ are n -unstable. Thus, the WSB of order n comprises all endpoints of each interval $[r_{2k-1}^*, r_{2k}^*]$

$$\partial W_n = \{r_k^*(\theta, e) | \theta \in [0, 2\pi], e \in [0, 1)\}. \tag{16}$$

It should be remarked that ∂W_n^* defined by Equation (12) is a proper subset of the extended WSB ∂W_n .

In order to display the geometry of the WSB on the initial (r, θ) plane, we also define a subset of ∂W_n by fixing the eccentricity e

$$\partial W_n(e) = \{r_k^*(\theta, e) | \theta \in [0, 2\pi]\}. \tag{17}$$

Analogously, Definitions 1 and 2 for describing the weak stability and instability for spacecraft m_3 can be easily extended to the PBR4BP, just with one more unstable condition added, i.e. m_3 collides with Jupiter. Consequently, we can obtain the refined weakly n -stable sets and their WSBs, by introducing the gravitational perturbation of Jupiter on m_3 .

4 COMPUTATION OF WEAKLY STABLE SETS

According to the algorithmic definition given in Section 3, to determine the weakly stable/unstable points around Mars, we have to integrate a large number of trajectories starting on the radial segment $l(\theta)$ with the initial velocity vector that is normal to it. For a fixed eccentricity $e \in [0, 1)$ (i.e. $H_2(0) < 0$), we have the initial conditions of the spacecraft at the time $t = 0$

$$\begin{aligned} x(0) &= 1 - \mu + r \cos \theta, & y(0) &= r \sin \theta, \\ \dot{x}(0) &= -v \sin \theta + r \sin \theta, & \dot{y}(0) &= v \cos \theta - r \cos \theta, \end{aligned} \tag{18}$$

where the position and velocity are in the framework of the synodic system (x, y) .

As $\theta_2(t)$ stands for the polar angle that the position vector of m_3 relative to m_2 makes with the positive direction of the x -axis, then we have $\theta_2(0) = \theta$. By integrating the equations of motion (1) or (7), we can track the time evolution of $\theta_2(t)$ through the trigonometric relations

$$\cos \theta_2 = \frac{x - 1 + \mu}{r_2} \quad \text{and} \quad \sin \theta_2 = \frac{y}{r_2}. \tag{19}$$

However, the value of $\theta_2(t)$, determined by this procedure, will vary within the limited range $[0, 2\pi]$ and discontinuously across $\theta_2 = 2\pi$. In order to verify whether m_3 completes n full cycles around m_2 at $t = t_n$ by a simple criterion

$$|\theta_2(t_n) - \theta| = n \cdot 2\pi, \tag{20}$$

it is natural to consider the dynamical system in polar coordinates (r_2, θ_2) relative to m_2 , where $\theta_2(t)$ turns out to be a monotonic increasing function of time t .

4.1 WSB in the PCR3BP

In this subsection, we will draw on some formulas deduced in the previous work of Topputo & Belbruno (2009). In the m_2 -centered polar reference system, the coordinates (r_2, θ_2) are defined by

$$x = 1 - \mu + r_2 \cos \theta_2, \quad y = r_2 \sin \theta_2, \quad (21)$$

and the equations of motion (1) for m_3 can be written explicitly as

$$\begin{aligned} \ddot{r}_2 - r_2 \dot{\theta}_2^2 - 2r_2 \dot{\theta}_2 &= (1 - \mu) \cos \theta_2 \left(1 - \frac{1}{r_1^3}\right) + r_2 \left(1 - \frac{1 - \mu}{r_1^3}\right) - \frac{\mu}{r_2^2}, \\ r_2 \ddot{\theta}_2 + 2\dot{r}_2 \dot{\theta}_2 + 2\dot{r}_2 &= (1 - \mu) \sin \theta_2 \left(\frac{1}{r_1^3} - 1\right), \end{aligned} \quad (22)$$

with initial conditions

$$\begin{aligned} r_2(0) &= r, \quad \theta_2(0) = \theta, \\ \dot{r}_2(0) &= 0, \quad \dot{\theta}_2(0) = \sqrt{\frac{\mu(1+e)}{r^3}} - 1. \end{aligned} \quad (23)$$

In the same manner, to check whether the spacecraft makes a full cycle around the Sun, we also introduce the m_1 -centered polar reference system. The coordinates (r_1, θ_1) are related to the Cartesian coordinates (x, y) through

$$x = -\mu + r_1 \cos \theta_1, \quad y = r_1 \sin \theta_1, \quad (24)$$

and then Equation (1) becomes

$$\begin{aligned} \ddot{r}_1 - r_1 \dot{\theta}_1^2 - 2r_1 \dot{\theta}_1 &= \mu \cos \theta_1 \left(\frac{1}{r_2^3} - 1\right) + r_1 \left(1 - \frac{\mu}{r_2^3}\right) - \frac{1 - \mu}{r_1^2}, \\ r_1 \ddot{\theta}_1 + 2\dot{r}_1 \dot{\theta}_1 + 2\dot{r}_1 &= \mu \sin \theta_1 \left(1 - \frac{1}{r_2^3}\right), \end{aligned} \quad (25)$$

with initial conditions

$$\begin{aligned} r_1(0) &= \sqrt{r^2 + 2r \cos \theta + 1}, \quad \theta_1(0) = \tan^{-1} \left(\frac{r \sin \theta}{1 + r \cos \theta} \right), \\ \dot{r}_1(0) &= -r \dot{\theta}_2(0) \sin(\theta - \theta_1(0)), \quad \dot{\theta}_1(0) = \frac{r \dot{\theta}_2(0)}{r_1(0)} \cos(\theta - \theta_1(0)). \end{aligned} \quad (26)$$

By solving the coupled systems (22) and (25) simultaneously, we are able to produce both angles θ_2 and θ_1 as smooth functions of time. Then we say that the motion of m_3 is weakly n -stable if the condition (20) is fulfilled, and the Kepler energy $H_2 \leq 0$ at each intersection of its trajectory with l , and m_3 has not completed a revolution around m_1 , i.e. $|\theta_1(t_n) - \theta_1(0)| < 2\pi$.

The weakly n -stable sets $W_n(e)$ have been numerically computed at six values of the eccentricity given by $e = 0.0, 0.2, 0.4, 0.6, 0.8, 0.95$. For the initial radius r and azimuth θ , we choose a reasonably high resolution of $\Delta r = 20\,000$ km ($\approx 8.8 \times 10^{-4}$ in adimensional units) and $\Delta \theta = 1^\circ$. Slightly different from previous works starting from $r = 0$, the minimum value of r is set to be 5000 km, which is a bit larger than Mars's physical radius (≈ 3396 km). The maximum radius r is taken to be one Sun-Mars distance, about 2.28×10^8 km (i.e. 1 in the adimensional unit system).

We employed a 7-8th-order Runge-Kutta-Fehlberg algorithm with an adaptive stepsize, and local truncation error as small as 10^{-20} . The span of integration time is set to be equal to 200π in adimensional time units, which corresponds to 100 orbital periods for Mars. After this time interval,

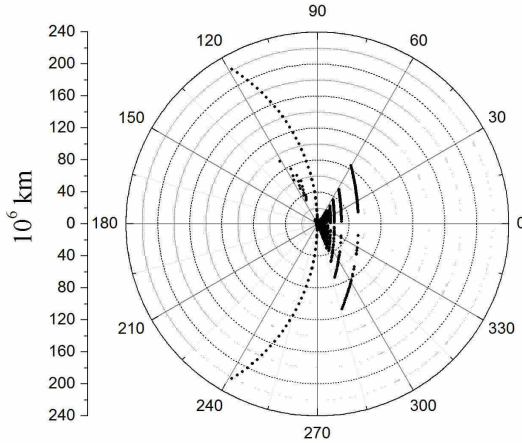


Fig. 3 A global view of the weakly 1-stable set $W_1(0.0)$ for the radius r as large as one Sun-Mars distance ($\sim 2.28 \times 10^8$ km) in the PCR3BP. The origin of the polar reference system is located at Mars (m_2).

if m_3 has not performed n complete turns around m_2 , the motion is classified as unstable. For the sake of detecting a collision between the spacecraft and the surface of any primary, the regularization transformation has not been included in our codes, and the numerical integration of an orbit would be terminated early if $r_2 \leq R_{\text{Mars}}$ or $r_1 \leq R_{\text{Sun}}$ (or $r_J \leq R_{\text{Jupiter}}$ in the later PBR4BP), where R is the physical radius of an object.

Figure 3 reports our preliminary results of weakly stable sets $W_n(e)$ in the Sun-Mars system for the case of $n = 1$ and $e = 0.0$. The geometry of $W_1(0.0)$ can be divided into three major parts: (1) the domain close to Mars; (2) two curves extending as far as one Sun-Mars distance, but they comprise a series of discrete stable points; (3) the region from $\theta = -75^\circ$ to 60° , where there are multiple transitions from stability to instability, and the stable set along each radial segment l possesses a Cantorian structure. These arc-like stable sets have not been observed in the Sun-Jupiter system or the Earth-Moon system, as we discuss below.

The global geometry of the stable set $W_1(0.0)$ obtained here is clearly different from that shown in previous studies (García & Gómez (2007); Romagnoli & Circi 2009; Topputo & Belbruno 2009), in the sense that the Sun-Mars system has an extremely small mass ratio ($\mu = 3.2271504036 \times 10^{-7}$) compared to both the Earth-Moon case ($\mu_{\text{EM}} = 1.2150585609 \times 10^{-2}$) and the Sun-Jupiter case ($\mu_{\text{SJ}} = 0.9538811803 \times 10^{-3}$). This can be understood by looking at the equations of motion (1), where the mass ratio is the only parameter. Indeed, if considering only the first stable/unstable transition, the set ∂W_n^* can be approximately represented by the surface of section $C(r, \theta, e) = C_{L_1}$ in space (r, θ) for a fixed value of e (Belbruno 2002). As ∂W_n^* is the boundary of the core of the stable set W_n in the case of multiple transitions, we propose that the relative size of W_n could be characterized by the Hill radius

$$r_H = \left(\frac{\mu}{3}\right)^{1/3}, \tag{27}$$

which denotes the adimensional distance from m_2 to the Lagrangian equilibrium point L_1 (Fig. 1).

Taking into account the amplification factor $(\mu_{\text{EM}}/\mu)^{1/3} \approx 34$, an enlarged view of the weakly stable region in the neighborhood of Mars is shown in Figure 4, for different values of the eccentricity e . As is clearly seen, with four arms extending from the four corners of the central stable core close

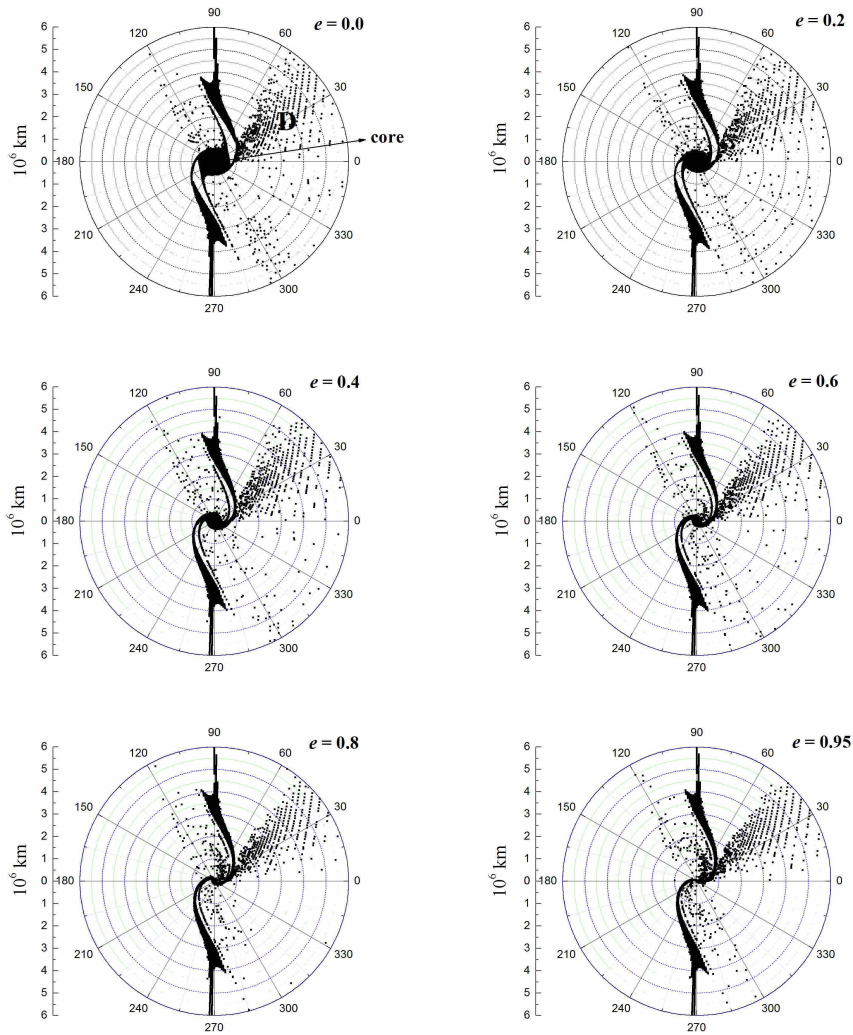


Fig. 4 Weakly 1-stable sets $W_1(e)$ for eccentricities $e = 0.0, 0.2, 0.4, 0.6, 0.8, 0.95$ in the PCR3BP, with an enlarged view of the domain relatively close to Mars.

to Mars, respectively, the main structure of the scaled 1-stable sets $W_1(e)$ is similar to the Earth-Moon case (Romagnoli & Circi 2009); and the contraction of the stable core with increasing e has also been identified. Likewise, our results can also be scaled to the Sun-Jupiter case by using the amplification factor $(\mu_{SJ}/\mu)^{1/3}$.

We recall that, in the case of $n = 1$ and $e = 0.0$, Figure 3 shows the arc-like stable sets in the region from $\theta = -75^\circ$ to 60° . This very structure has been magnified in the upper left panel of Figure 4, while the overwhelming majority of stable points reside in the sectorial area $\theta \in (0, 60^\circ)$, which is recorded as Sector-D. Compared with the cases of the Earth-Moon and Sun-Jupiter, Sector-D represents a new stable regime about m_2 in the PCR3BP for the extremely small mass ratio of the primaries.

As illustrated, the surface of section $C = C_{L_1}$ represents an analytic approximation of $\partial W_1^*(0,0)$, i.e. the boundary of the core of $W_1(0,0)$, out of which all the stable trajectories have Jacobi constant values smaller than C_{L_1} . Hence, the four arms and Sector-D are of particular interest since for $C < C_{L_1}$ two branches of the zero velocity curves around m_1 and m_2 are connected through a neck opened at L_1 , such that ballistic capture can take place. Furthermore, as shown in Figure 4, the geometric configurations of the arms and Sector-D would barely change, even when the eccentricity goes to 1.

It is important to note that our aim is to explore the WSB transfer by which the spacecraft can approach a domain near Mars, hence only the ballistic capture for a not too large perimartian altitude is worth studying further. From now on, we will investigate the weak stability problem using the same scale as in Figure 4 that covers a relatively small initial distance r from Mars.

4.2 WSB in the PBR4BP

A more realistic model for computation of the Martian WSB is represented by the PBR4BP, in which the gravitational perturbation from Jupiter on the motion of the spacecraft is included. For the reasons given at the beginning of Section 4, we will establish the equations of motion in polar coordinates for the PBR4BP.

In the m_2 -centered polar reference system, the set of differential equations given in Equation (22) is modified as

$$\begin{aligned} \ddot{r}_2 - r_2 \dot{\theta}_2^2 - 2r_2 \dot{\theta}_2 &= (1-\mu) \cos \theta_2 \left(1 - \frac{1}{r_1^3}\right) + r_2 \left(1 - \frac{1-\mu}{r_1^3}\right) - \frac{\mu}{r_2^2} + f_2 \cos \theta_2 + g_2 \sin \theta_2, \\ r_2 \ddot{\theta}_2 + 2\dot{r}_2 \dot{\theta}_2 + 2\dot{r}_2 &= (1-\mu) \sin \theta_2 \left(\frac{1}{r_1^3} - 1\right) - f_2 \sin \theta_2 + g_2 \cos \theta_2, \end{aligned} \quad (28)$$

where

$$\begin{aligned} f_2(r_2, \theta_2) &= -m_J \left(\frac{r_2 \cos \theta_2 + 1 - \mu - \rho \cos \phi}{r_J^3} + \frac{\cos \phi}{\rho^2} \right), \\ g_2(r_2, \theta_2) &= -m_J \left(\frac{r_2 \sin \theta_2 - \rho \sin \phi}{r_J^3} + \frac{\sin \phi}{\rho^2} \right). \end{aligned} \quad (29)$$

Analogously, the coupled system defined by Equation (25) relative to m_1 in polar coordinates turns out to be

$$\begin{aligned} \ddot{r}_1 - r_1 \dot{\theta}_1^2 - 2r_1 \dot{\theta}_1 &= \mu \cos \theta_1 \left(\frac{1}{r_2^3} - 1\right) + r_1 \left(1 - \frac{\mu}{r_2^3}\right) - \frac{1-\mu}{r_1^2} + f_1 \cos \theta_1 + g_1 \sin \theta_1, \\ r_1 \ddot{\theta}_1 + 2\dot{r}_1 \dot{\theta}_1 + 2\dot{r}_1 &= \mu \sin \theta_1 \left(1 - \frac{1}{r_2^3}\right) - f_1 \sin \theta_1 + g_1 \cos \theta_1, \end{aligned} \quad (30)$$

where

$$\begin{aligned} f_1(r_1, \theta_1) &= -m_J \left(\frac{r_1 \cos \theta_1 - \mu - \rho \cos \phi}{r_J^3} + \frac{\cos \phi}{\rho^2} \right), \\ g_1(r_1, \theta_1) &= -m_J \left(\frac{r_1 \sin \theta_1 - \rho \sin \phi}{r_J^3} + \frac{\sin \phi}{\rho^2} \right). \end{aligned} \quad (31)$$

Note that the initial conditions of both systems in Equations (28) and (30) are exactly the same as in the PCR3BP, given by Equations (23) and (26), respectively.

In the framework of the PBR4BP, we have done the following numerical experiments to better understand properties of the weakly n -stable sets $\tilde{W}_n(e)$ and their boundaries, for different values of the eccentricity e , the initial phase angle ϕ_0 of Jupiter and the stability number n .

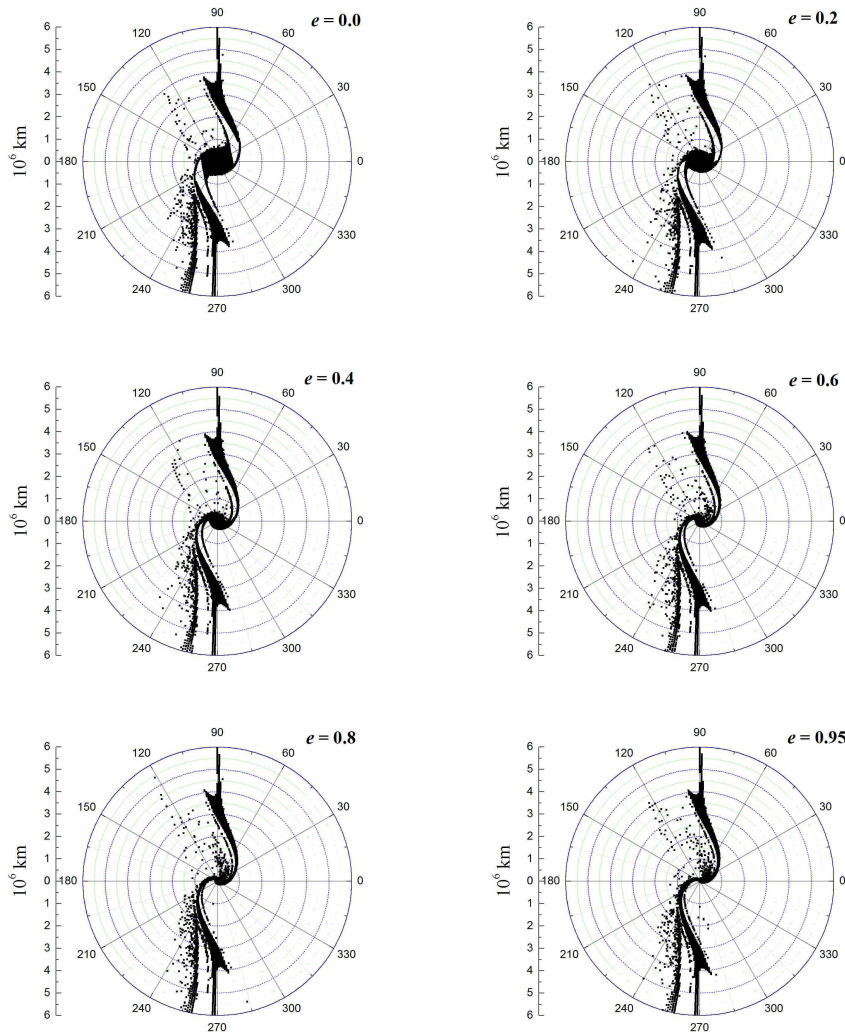


Fig. 5 Weakly 1-stable sets $\tilde{W}_1(e)$ for increasing e in the framework of the PBR4BP. It can be seen that the stable Sector-D presented in the PCR3BP disappears, while a new stable branch is derived from the lower left arm.

4.2.1 Structure of 1-stable sets

Figure 5 displays the behavior of the weakly 1-stable sets $\tilde{W}_1(e)$ for increasing values of e in the PBR4BP. Comparing Figure 5 against Figure 4, it is immediately found that the stable Sector-D presented in the PCR3BP disappears. Note that the Mars-Jupiter distance reaches its minimum when the phase angle $\phi = 0$ in the bicircular model, i.e. Jupiter lies on the radial segment $l(\theta = 0)$ outside the position of Mars. This implies that Sector-D with $\theta \in (0, 60^\circ)$ suffers the strongest perturbation from Jupiter and the points inside this region will lose their weak stabilities. Nevertheless, it can be observed that there is a new WSB branch derived from the lower left arm of $\tilde{W}_1(e)$ in the PBR4BP,

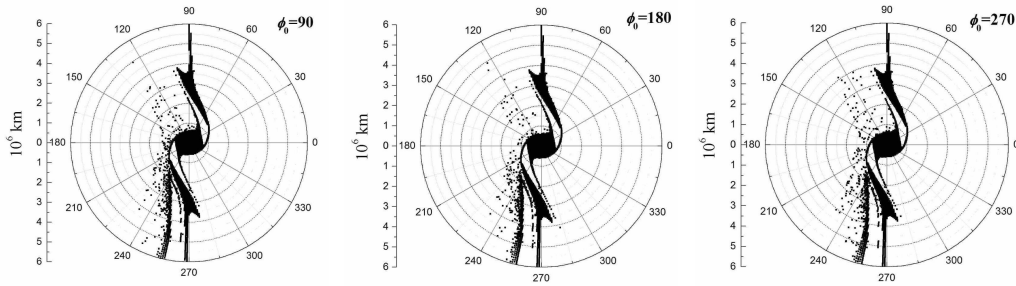


Fig. 6 Weakly 1-stable sets $\tilde{W}_1(0.0)$ for different values of the initial phase angle ϕ_0 of Jupiter. The case of $\phi_0 = 0$ has been shown in the upper left panel of Fig. 5.

extending from a fixed value of the azimuth $\theta^* = 210^\circ$. Moreover, even if the eccentricity increases to about 1, the geometry of this branch remains unchanged. Besides these two apparent discrepancies between the three and four body models, the overall configurations of $\tilde{W}_1(e)$ are almost identical for each fixed eccentricity.

In the above research for the PBR4BP case, we require that Jupiter starts its motion from the point in the positive direction of the x -axis, i.e. the initial phase angle $\phi_0 = 0$. As illustrated, the influence of Jupiter on the Martian WSB is relatively large under such a configuration. Since Mars and Jupiter are assumed to move on circular and non-resonant orbits, theoretically speaking, the cumulative effect of Jupiter's perturbation on the Sun-Mars system should be independent of ϕ_0 . However, for a large proportion of stable points plotted in Figure 5, they return to the radial line $l(\theta)$ within only one orbital period of Mars. During this time span, the angular displacement $\Delta\phi$ of Jupiter would be no greater than 57° . Thus, in order to have a complete view of the case where Jupiter is a perturbation, it is necessary to consider different initial positions of Jupiter relative to the Sun-Mars system.

In Figure 6, we graph the 1-stable sets $\tilde{W}_1(0.0)$ for the other three representative angles of $\phi_0 = 90^\circ, 180^\circ$ and 270° . Combining the result from the upper left panel of Figure 5 for the case of $\phi_0 = 0$, it is perfectly apparent that these stable sets are qualitatively the same. This suggests that the influence of Jupiter's initial phase could be neglected in the study of the WSB around Mars.

In the framework of the PBR4BP, all collisions take place at the surface of either Mars or the Sun, and no collisions with Jupiter have been observed for the time span of 100 orbital periods of Mars in our integrations.

4.2.2 The case of n -stability ($n \geq 2$)

Since we want to use the WSB to design low-energy transfer trajectories by the mechanism of ballistic capture, we must take into account the lifetime of the spacecraft around Mars. The period of a spacecraft orbiting Mars can be estimated by its perimartian altitude and eccentricity, then we may determine how many revolutions it should complete to accomplish the exploration task, i.e. with regard to the stability number n .

Once the 1-stable sets \tilde{W}_1 have been carried out in the PBR4BP, the next step is the computation of \tilde{W}_n corresponding to increasing order n . It is straightforward to verify that $\tilde{W}_n \subseteq \tilde{W}_m$ if $n > m$, for a fixed value of e . Therefore, we can use the initial conditions for $(n-1)$ -stability to generate n -stable sets. This trick saves a huge amount of CPU time, since all the weakly $(n-1)$ -unstable trajectories are excluded from the numerical calculations.

Starting with the stability number $n = 2$, we graphically produce a sequence of \tilde{W}_n up to $n = 9$. These stable sets are shown in Figures 7 and 8 for $e = 0$ and 0.95, respectively, associated

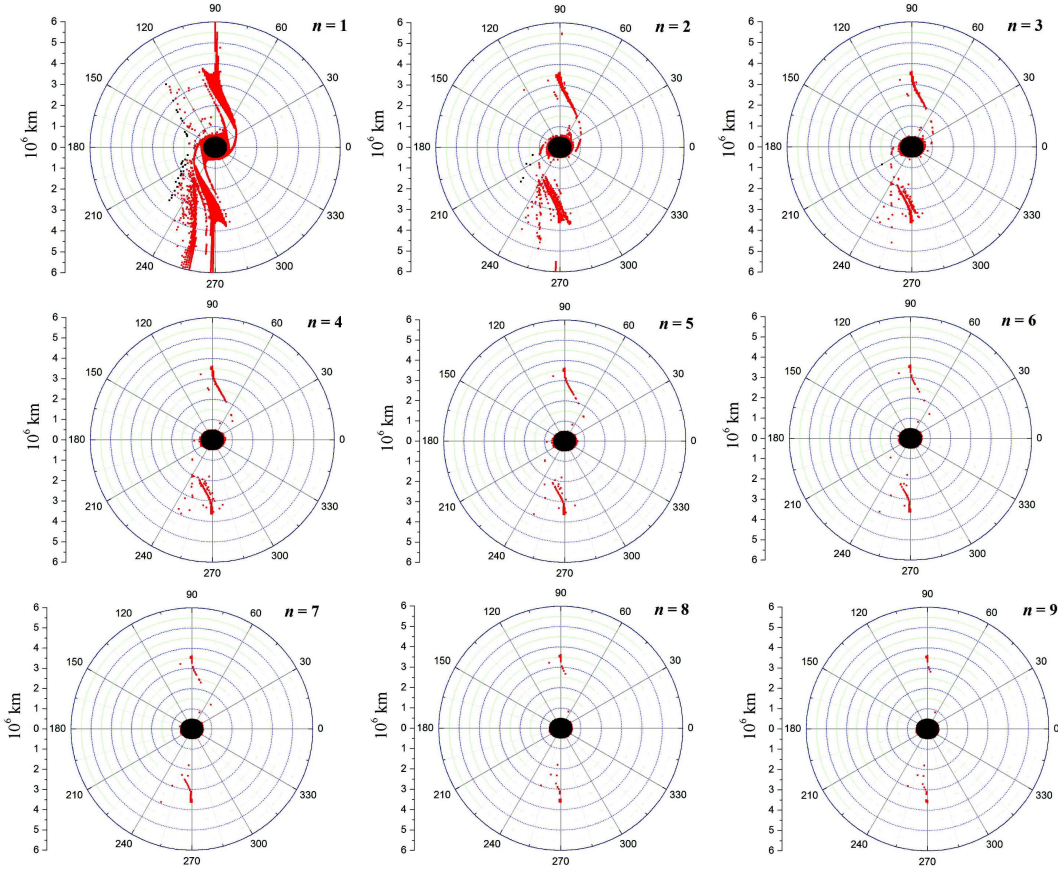


Fig. 7 The sequence of weakly n -stable sets $\tilde{W}_n(e)$ for the stability number $n = 1, 2, 3, 4, 5, 6, 7, 8, 9$ with $e = 0.0$ in the PBR4BP. The points with the initial Jacobi “constant” $C < C_{L_1}$ have been plotted in red (*color online*).

with the 1-stable sets $\tilde{W}_1(0.0)$ and $\tilde{W}_1(0.95)$ from Figure 5. In order to highlight the weakly n -stable points with $C < C_{L_1}$, which have properties that the zero velocity curves are open at L_1 and the ballistic capture transfer of the spacecraft into the Mars orbit is allowed, they have been plotted in red. However, for black stable points with $C \geq C_{L_1}$, there is no possibility for an orbital transfer since they correspond to trajectories that will be permanently bounded in the Hill region of Mars as $t \rightarrow \pm\infty$.

It is worth remarking that the value of C is not conserved in the PBR4BP. From Equations (5) and (7), we have

$$\frac{dC}{dt} = 2 \left(\frac{\partial \Omega}{\partial x} \cdot \dot{x} + \frac{\partial \Omega}{\partial y} \cdot \dot{y} \right) = 2 \left(\frac{d\Omega}{dt} - \frac{\partial \Omega}{\partial t} \right). \quad (32)$$

Then we integrate Equation (32) from 0 to t

$$\Delta C = 2 [\Omega(0) - \Omega(t)] + 2 \int_0^t \frac{\partial \Omega}{\partial t} dt. \quad (33)$$

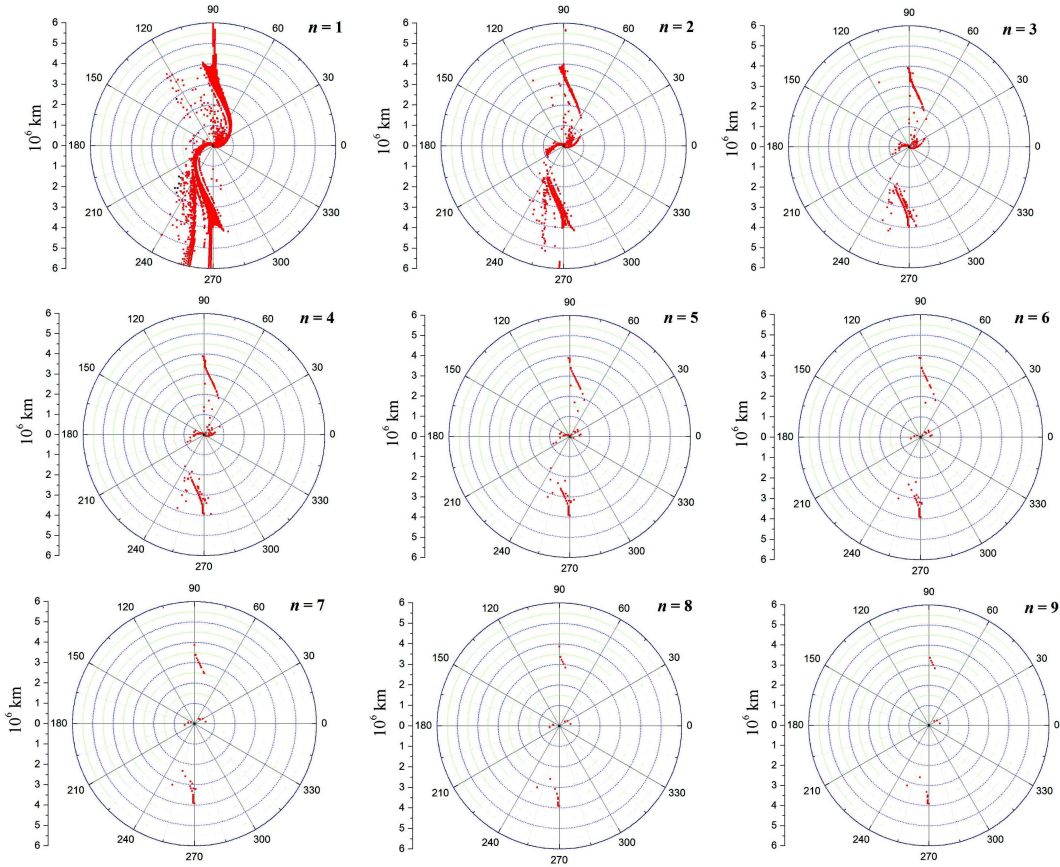


Fig. 8 Same as in Fig. 7, but for $e = 0.95$.

Since the integral in Equation (33) is defined relative to the evolution of the trajectory, we cannot analytically estimate this time variation of C . Nevertheless, a careful examination of all the stable trajectories over n revolutions reveals that ΔC turns out to be within $\sim 10^{-5}$ and is negligible. This suggests that the topology of the region of possible motion of m_3 , related to the WSB transfer, may be well constrained by studying the Jacobi “constant” in the PBR4BP.

In Figure 7, one can find that the (black) core of $\tilde{W}_1(0.0)$ is preserved as the stability number n increases, while all the (red) arms become more and more sparse. It is also seen that these arms exist in the form of a continuous structure for a certain range of n , and they end up in only a few discrete points when $n \geq 8$. As for the case of $e = 0.95$ with increasing n shown in Figure 8, the evolution of the geometry of the weakly stable regions is equivalent. The information about the n -stable sets may allow us to determine the initial conditions of a spacecraft leading to ballistic capture within its required lifetime around Mars.

5 CONCLUSIONS AND DISCUSSION

The WSB transfers require substantially less fuel for a spacecraft to be automatically captured by a target, such as the Moon or other planets and satellites in our Solar System, as compared to traditional Hohmann transfers. They are designed to eliminate the hyperbolic excess velocity at arrival, and are thus called ballistic capture. In this paper, we investigated the geometry of the WSBs around the

planet Mars, which is not only a new case but may also be very advantageous for future space missions.

First, we computed the WSB region in the Sun-Mars-spacecraft configuration by adopting the PCR3BP. It is seen that the relative size of the weakly stable sets is much larger than that of the Earth-Moon and the Sun-Jupiter systems, as the mass ratio of the Sun-Mars system is four to five orders of magnitude smaller. We propose that this difference could be characterized by the Hill radius of the second primary. Accordingly, an enlarged view of the domain close to Mars is presented. We find that the main structure of the stable sets, a core with four arms extending from its four corners, is approximately the same as in the cases of the Earth-Moon and Sun-Jupiter (García & Gómez 2007; Topputo & Belbruno 2009). Nevertheless, a new stable regime in the sectorial area $\theta \in (0, 60^\circ)$ appears; it is identified as Sector-D. For increasing values of the initial eccentricity e relative to Mars, the core of stable sets reduces in size, but the four arms and Sector-D would barely change even when e goes to 1.

Next, we take into account the influence of Jupiter on the Martian WSB, by means of the PBR4BP. On comparing with the PCR3BP case, we find that there are two apparent discrepancies: (1) Sector-D becomes totally unstable, since it is the very region that suffers the strongest gravitational perturbation from Jupiter; (2) there is a new continuous WSB branch derived from the lower left arm of the Sun-Mars stable sets, starting at a particular polar angle $\theta^* = 210^\circ$. Moreover, our numerical simulations show that these results are independent of the initial eccentricity e and the initial phase angle of Jupiter.

It should be noted that the above computations have been done for the weakly 1-stable sets, where the spacecraft is required to make only one complete circle around Mars. Finally, we further examined the structure of the n -stable ($n \geq 2$) sets in the framework of the PBR4BP. This study demonstrated that, for increasing values of the stability number n , the stable core could be very well preserved, but all the arms become more and more sparse, and they end up in only a few discrete points when $n \geq 8$. However, the appearance of these isolated stable points may not be intrinsic but due to the discontinuity in initial values of r and θ .

Aside from the Sun-Mars system considered in this paper, actually, another set of primaries with extremely small mass ratio has been pursued for the intriguing case of the Sun-Mercury (Makó et al. 2010). However, unlike any other planets in the Solar System, Mercury has a substantial orbital eccentricity of > 0.2 . Thus Makó et al. computed the WSB around Mars in the framework of the elliptic restricted 3-body problem, where the two primaries are moving on elliptic orbits. Such an eccentric celestial system may be further extended in some restricted 4-body model by including the perturbation of the planet Venus, to better construct Mercury's WSB and especially the low-energy transfer trajectories.

Acknowledgements This work was supported by the National Natural Science Foundation of China (Grant Nos. 11473015, 11333002, 11178006 and 11078001), the National Basic Research Program of China (973 program, 2013CB834103), the 985 project of Nanjing University and the Advanced Discipline Construction Project of Jiangsu Province.

References

- Bate, R. R., Mueller, D. D., & White, J. E. 1971, *Fundamentals of Astrodynamics*, eds. Bate, R. R., Mueller, D. D., White, J. E. (New York: Dover Publications)
- Belbruno, E. A., ed. 1987, in *AIAA/DGLR/JSASS International Electric Propulsion Conference*, 19th, AIAA Paper No. 87-1054
- Belbruno, E., & Miller, J. 1990, *Jet Propulsion Laboratory, IOM*, 312, 90
- Belbruno, E. A., & Miller, J. K. 1993, *Journal of Guidance Control Dynamics*, 16, 770

- Belbruno, E. A., & Carrico, J. P. 2000, in AIAA/AAS Astrodynamics Specialist Conference, AIAA Paper No. 2000-4142
- Belbruno, E. 2002, *Contemporary Mathematics*, 292, 17
- Belbruno, E. 2004, *Capture Dynamics and Chaotic Motions in Celestial Mechanics: With Applications to the Construction of Low Energy Transfers* (Princeton: Princeton University Press)
- Belbruno, E., Gidea, M., & Topputo, F. 2010, *SIAM Journal on Applied Dynamical Systems*, 9, 1061
- García, F., & Gómez, G. 2007, *Celestial Mechanics and Dynamical Astronomy*, 97, 87
- Hill, G. W. 1878, *American Journal of Mathematics*, 1, 5
- Hohmann, W. 1925, *Die Erreichbarkeit der Himmelskörper. Untersuchungen über das Raumfahrtproblem* (Munich: Oldenbourg)
- Jehn, R., Campagnola, S., Garcia, D., & Kemble, S. 2004, in 18th International Symposium on Space Flight Dynamics, ESA Special Publication, 548, 487
- Makó, Z., Szenkovits, F., Salamon, J., & Oláh-Gál, R. 2010, *Celestial Mechanics and Dynamical Astronomy*, 108, 357
- Murray, C. D., & Dermott, S. F. 1999, *Solar System Dynamics* (New York: Cambridge Univ. Press)
- Romagnoli, D., & Circi, C. 2009, *Celestial Mechanics and Dynamical Astronomy*, 103, 79
- Schoenmaekers, J., Horas, D., & Pulido, J. 2001, in 16th International Symposium on Space Flight Dynamics, Pasadena, California, 114
- Sousa Silva, P. A., & Terra, M. O. 2012a, *Celestial Mechanics and Dynamical Astronomy*, 113, 141
- Sousa Silva, P. A., & Terra, M. O. 2012b, *Celestial Mechanics and Dynamical Astronomy*, 113, 453
- Szebehely, V. 1978, *Celestial Mechanics*, 18, 383
- Topputo, F., & Belbruno, E. 2009, *Celestial Mechanics and Dynamical Astronomy*, 105, 3
- Yagasaki, K. 2004a, *Celestial Mechanics and Dynamical Astronomy*, 90, 197
- Yagasaki, K. 2004b, *Physica D Nonlinear Phenomena*, 197, 313